Alteration of the Mechanical and Thermal Properties of Nylon 6/Nylon 6,6 Blends by Nanoclay

Rabab Jarrar,[1] Mahmood A. Mohsin,[2] Yousef Haik[1,3]

[1]*Center for Research Excellence in Nanobiosciences, University of North Carolina at Greensboro, Greensboro, North Carolina 27412*
[2]*Department of Chemistry, United Arab Emirates University, P. O. Box 17551, Al Ain, United Arab Emirates*
[3]*Department of Mechanical Engineering, United Arab Emirates University, P. O. Box 17555, Al Ain, United Arab Emirates*

Received 12 April 2010; accepted 8 July 2011
DOI 10.1002/app.35215
Published online 24 October 2011 in Wiley Online Library (wileyonlinelibrary.com).

ABSTRACT: Nylon 6 [N(6)], nylon 6,6 [N(6,6)], and their blends at different clay loadings were prepared. The mix was melted and injected into strip-shaped samples. Mechanical and thermal analyses were performed to investigate the effect of blending and the incorporated clay on the mechanical and thermal properties. Enhancements in the Young's modulus and hardness were obtained for all of the nanocomposites, with a 55% increase in Young's modulus after the addition of 6 wt % nanoclay, although the improvement in tensile strength depended on the blend ratio, with greatest effects on the 50% N(6)/50% N(6,6) blend with increases of 44 and 59% for 2 and 4% clay loadings, respectively. Thermogravimetric analysis showed an enhancement in the thermal properties in the 50% N(6)/50% N(6,6) blend at 2% clay loading, and the blend exhibited ductile behavior at this loading. Increases in the crystallization peak temperatures of 10–15° in N(6,6) and the two blends 30% N(6)/70% N(6,6) and 50% N(6)/50% N(6,6) were observed after the addition of the clay. The nanoclay enhanced the γ-/β-form crystals in N(6) and N(6,6) neat polymers and also in the blends. Fourier transform infrared spectroscopy FT-IR revealed the formation of hydrogen bonding and the possible formation of ionic bonds between the polymers and the nanoclay, which resulted in enhancements in the mechanical properties of the blends. The distribution of the nanoclay in the blend was well dispersed, as shown by X-ray diffraction analysis. © 2011 Wiley Periodicals, Inc. J Appl Polym Sci 124: 1880–1890, 2012

Key words: clay; FT-IR; mechanical properties; nanocomposites; thermal properties

INTRODUCTION

The use of nanoclay to raise polymers to new capabilities has been widely investigated in the last 2 decades. The addition of a nanoclay to a polymer matrix improves its physical properties at very low loadings in comparison with conventional fillers. This savings in weight and the improvements in the physical properties make the nanocomposite technology commercially applicable.

Many researchers have studied the effects of nanoclay on polymers on the basis of single polymer matrixes, including nylon 6,6 [N(6,6)],[1,2] nylon 6 [N(6)],[3–5] polypropylene (PP),[6,7] polystyrene,[8,9] and others.

N(6) is one of the polymers for which well-exfoliated nanocomposites have been achieved with several processing routes, and N(6,6) is an engineering polymer with many useful and interesting applications.

N(6) is usually synthesized by a ring-opening polymerization of ε-caprolactam monomer to produce a polyamide in which the repeating unit is given in Scheme 1, together with N(6,6), which is commercially prepared by the step-growth polymerization between diamine (hexamethylene diamine) and dicarboxylic acid (adipic acid).

The mixing of polymers has become commercially and technologically more important than the fabrication of homopolymers and copolymers in the last decade. Blending allows one to create new materials from a wide range of existing materials with specific properties for the desired application at low cost.

There are few reports involving blend nanocomposites. Wahit et al.[10] studied the effects of organoclay and ethylene–octene copolymer on the morphology and mechanical properties of polyamide/PP blends. They found that the blend ratio and presence of organoclay influenced the morphology of the nanocomposites. Tiwari and Khilar[11] studied the thermal and mechanical properties of a new poly (phenylene oxide)/polystyrene blend. An improvement in the tensile modulus was observed in comparison to the blend, whereas decreases in the tensile strength and elongation were observed with increases in the clay loading. Blend nanocomposites of PP and ethylene–propylene–diene rubber were

Correspondence to: R. Jarrar (rabab_jarrar@yahoo.com).

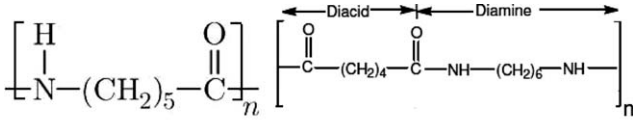

Scheme 1 Repeating unit of (a) N(6) and (b) N(6,6) showing the main functional groups.

prepared by a solvent blending method by Frounchi et al.[12] They reported an increase in the barrier properties, a decrease in the crystallinity, and consistency in the melting temperature after the addition of montmorillonite-based organoclay.

In this work, we aimed to investigate the effect of blending and effect of incorporated clay on the mechanical–thermal properties of N(6), N(6,6), and their blend composites.

EXPERIMENTAL

Materials

N(6) and N(6,6) where obtained from Fisher Scientific (Suwanee, GA) and were used without further modification. Their repeating units are given in Scheme 1, in which the degrees of polymerization are 100 and 200, respectively. A surface-modified montmorillonite nanoclay (1.34TCN nanomer) with 25–30 wt % methyl dihydroxyethyl hydrogenated tallow ammonium was obtained from Sigma Aldrich (St. Louis, MO) and was also used without modification.

Nanocomposite preparation

To ensure ideal mixing between N(6), N(6,6), and the nanoclay, we refined both N(6) and N(6,6) pellets to a powder form by cooling the pellets in liquid nitrogen and then crushing the cooled pellets using a high-speed blender for 10 min or until a very smooth and uniform powder was obtained. The composites and blends used in this work are described in Table I.

Mechanical measurements

Tensile testing

The composites were prepared by melting the specific formulation of the blend in an Haake injection-molding apparatus (Norwood Instruments, Ltd., Honley, England) with a nozzle diameter of 3 mm and an injection speed of 20 mm/s. The barrel temperature was adjusted to 228°C for N(6) and 264°C for N(6,6). The samples were produced in strip shapes 10 cm long, 1 cm wide, and 3 mm thick. Four samples were produced for each composite/blend formulation. The mechanical properties of the formed strips were tested with a universal tensile testing machine (MTS; 20/MH) equipped with a 5-kN standard load cell and with a crosshead speed of 10 mm/min. The system was equipped with universal testing software (TestWorks, San Francisco, CA). The average of three tested samples was used in the evaluation.

Indentation testing

Nanoindentation tests were performed on a Nano Test Materials testing platform (Micro Materials, Ltd., Wrexham, United Kingdom), which was equipped with a three-sided pyramid diamond indenter tip (Berkovich type). The nanoindentations were carried out at a constant displacement rate of 0.0167 nm/s to avoid strain-hardening effects on the

TABLE I
Mechanical and Thermal Properties Deduced from Tensile and Thermal Tests for N(6), N(6,6), and Their Nanocomposite Blends

Sample	Elongation at break (%)	Tensile strength (MPa)	Young's modulus (GPa)	T_{cry} (°C)	T_m (°C)
100% N(6)	18.00	59.9	1.376	187.4	220.0
4% clay	6.33	61.8	1.469	185.8	220.3
6% clay	4.44	66.9	2.136	184.2	218.7
100% N(6.6)	6.05	65.2	1.667	217.9	258.0
4% clay	8.70	70.1	1.800	227.4	260.2
6% clay	5.92	60.9	1.819	227.4	260.3
30% N(6)/70% N(6.6)	4.93	58.2	1.636	207.8	241.4
4% clay	5.33	58.5	1.648	212.9	244.3
6% clay	6.70	58.0	1.705	208.7	242.7
50% N(6)/50% N(6.6)	3.34	39.8	1.599	175.7	209.9
2% clay	5.60	57.4	1.566	186.3	226.6
4% clay	6.28	63.2	1.686	184.4	227.6
6% clay	4.46	49.8	1.704	184.5	230.5
70% N(6)/30% N(6.6)	3.30	40.1	1.618	177.2	211.0
4% clay	4.10	49.7	1.713	176.0	211.0
6% clay	4.52	49.0	1.742	174.8	210.1

measurement until a maximum depth of 1827 nm was reached. The load (1 mN) was held constant for 30 s to avoid creep, which can affect the unloading behavior. The indenter was then withdrawn from the surface at the same rate until 10% of the maximum load was reached; then, the indenter was completely removed from the material. Five indents were performed for each composite/blend sample. The distance between indentations was 50 μm to avoid interaction. The hardness and elastic modulus were calculated from the load–displacement data. As the indenter was allowed to penetrate into the specimen, both elastic and plastic deformation occurred, and only the elastic portion of the displacement was recovered during unloading. The slope (S) at the maximum load point (dP/dh) was the experimentally measured stiffness of the upper portion of the unloading data (Oliver–Pharr method),[13] which could be used to calculate the reduced modulus of elasticity (E_r) with the following equation:

$$E_r = \frac{S\sqrt{\pi}}{2\beta\sqrt{A_p}} \quad (1)$$

where A_p is the area of indentation at the contact depth, β is a constant that depends on the geometry of the indenter (β = 1.034 for a Berkovich indenter), and E_r is a combination of the sample material and indenter elastic deformations.[14,15] The effects of nonrigid indenters on the load–displacement behavior was taken into consideration through the definition of E_r through the following equation:

$$\frac{1}{E_r} = \frac{1-\nu_s^2}{E_s} + \frac{1-\nu_i^2}{E_i} \quad (2)$$

where E_s and ν_s are the Young's modulus and Poisson's ratio, respectively, for the sample. Poisson's ratio was taken to be 0.35 for N(6) and 0.41 for N(6,6) and between 0.35 and 0.41 for the blends. For the diamond indenter, the Young's modulus (E_i) was 1140 GPa, and Poisson's ratio (ν_i) was 0.07.

The area of contact at peak load was determined by the geometry of the indenter and the depth of contact.[13]

Thermal measurements

The thermal properties of the nanocomposites of N(6), N(6,6), and their blends were determined by differential scanning calorimetry (DSC) and thermogravimetric analysis (TGA).

The DSC measurements were performed on a TA Instruments DSC 200 (New Castle, DE) under a nitrogen atmosphere with a sample purge flow of 50 mL/min. About 10 mg of the polymer or the composite sample was used each time and was placed in a sealed aluminum pan to measure the peak melting temperature and crystallization temperature. In each run, the test samples were heated to 350°C at a heating rate of 10°C/min to eliminate any residual or thermal history acquired during sample preparation in the injection-molding machine. Then, they were cooled to 0°C at a rate of 10°C/min and heated again at the same rate to 350°C.

The TGA measurements were performed with a TA Instruments TGA Q500 under a nitrogen atmosphere with a balance purge flow of 40 mL/min and a sample purge flow of 60 mL/min. About 30 mg of the polymer sample was used each time. The measurements were done with a heating rate of 10°C/min in the temperature range from ambient to 600°C. The temperatures at 10% weight loss ($T_{90\%}$) and 50% weight loss ($T_{50\%}$), the residue percentage for the nanocomposite, and the maximum degradation rate were determined with TA Universal Analysis 2000 version 4.5A build 4.5.05 software (TA Instruments).

Fourier transform infrared (FTIR) spectroscopy

Transmission infrared spectra of all of the samples were recorded at room temperature with an FTIR spectrophotometer (NEXUS-470, Thermo Nicolet Corp. Vernon Hills, IL) in the wave- number range from 4000 to 400 cm^{-1} for 32 scans with a 2-cm^{-1} resolution. Granules of each sample were mixed in a ratio of 1.0 wt % with KBr powder dried at 120°C for 24 h. The mixture was milled to a fine powder and placed in the mold under hydraulic pressure to from a KBr disc. The sample disc was mounted directly onto the sample holder, and data for the spectra were collected after the background was scanned.

X-ray diffraction (XRD) analysis

XRD is the most common and simplest method for the morphological analysis of nanocomposites. XRD patterns of the blend samples were recorded with an Oxford Diffraction-Gemini diffractometer NoidaSEZ, India equipped with an area detector and operating at a voltage of 40 kV and a current of 40 mA with Cu Kα radiation (λ = 1.5406 nm) with range of angles (2θ's) from 0 to 120° and a step of 0.02° at 2 s/step. The d-spacing corresponding to the large peak was calculated from Bragg's equation:

$$\lambda = 2d\sin\theta$$

where 2θ is the X-ray scattering angle. A commercial curve-fitting module was used for data analysis. The changes in the interlayer spacing of the nanoclays

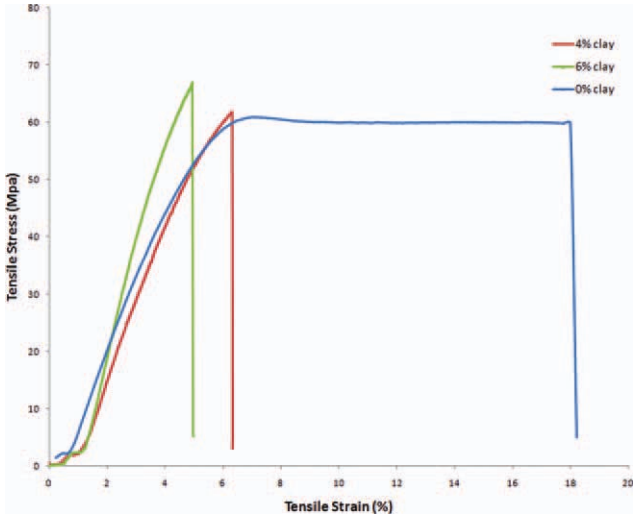

Figure 1 Stress–strain curves for N(6) nanocomposites containing 0, 4, and 6 wt % nanoclay. [Color figure can be viewed in the online issue, which is available at wileyonlinelibrary.com.]

were calculated with Bragg's law to determine the extent of exfoliation or intercalation in the nanocomposites.

RESULTS AND DISCUSSION

Tensile properties of the N(6)/N(6,6) blend nanocomposites

The mechanical properties of the different polymer nanocomposites were compared for the same blend ratio of N(6) to N(6,6) at different nanoclay contents. Figure 1 shows the representative stress–strain curves for neat N(6) with 4 and 6 wt % loadings of 1.34TCN. Figure 2 shows the stress–strain curve for the blends of 50% N(6) and 50% N(6,6) loaded with 0, 2, 4, and 6% nanoclay.

The Young's modulus, tensile strength, and elongation at break for all blend nanocomposites, which were obtained from the stress–strain curves (obtained by the averaging of the results of three samples), are summarized in Table I (data from DSC are also included). The Young's moduli for the neat blend composites were between those of the neat N(6) and N(6,6) and decreased with increasing N(6) loading. The addition of the nanoclay caused an increase in Young's modulus of all the nanocomposites over the neat polymers and their blend. This was in agreement with the behavior of other polymer nanocomposites reported in the literature,[16,17] but the amount of increase differed from one composite to other, having its greatest value for N(6) after the addition of 6 wt % nanoclay, with an increase of nearly 55% above its original value, although a slight increase in the modulus of only 6% was detected for the 50 wt % N(6)/50 wt % N(6,6) blend after the addition of the same amount of nanoclay. The enhancement of Young's modulus was due to the reinforcement of the dispersed layers of the nanoclay and to the good interaction of the clay with the N(6) matrix.[1]

The tensile strengths of the neat N(6) and neat N(6,6) were greater than those of their neat blends. The effect of the addition of nanoclay on the tensile strength depended on the blend ratio of the composite, with the greatest effect on the 50 wt % N(6)/50 wt % N(6,6) blend. The tensile strength of this blend increased by an amount of 44% for 2 wt % clay loading and by 59% for 4 wt % clay loading, and this increase was followed by a decrease for the loading of 6 wt %, which was still greater than the value of the neat blend, so this behavior of the tensile strength (an increase followed by a decrease) after certain loadings of clay was exhibited by N(6,6), whereas it remained constant beyond 4 wt % clay content for the 30 wt % N(6)/70 wt % N(6,6) and 70 wt % N(6)/30 wt % N(6,6) blends. Nanoclay-containing polymeric nanocomposites encompass a number of advantages over conventional composites. The main improvements are in the modulus, hardness, impact strength, heat resistance, and dimensional and thermal stabilities. The addition of a few percentage of nanoclay can enhance these properties, but the addition of more nanoclay may not necessarily produce more improvement in the mechanical properties. This is due to the increase in the viscosity of the polymer with the addition of nanoclay and the intensification of the amount of air bubbles produced during the mixing process. The addition of a large percentage of nanoclay tended to cause agglomeration, which caused a constancy or

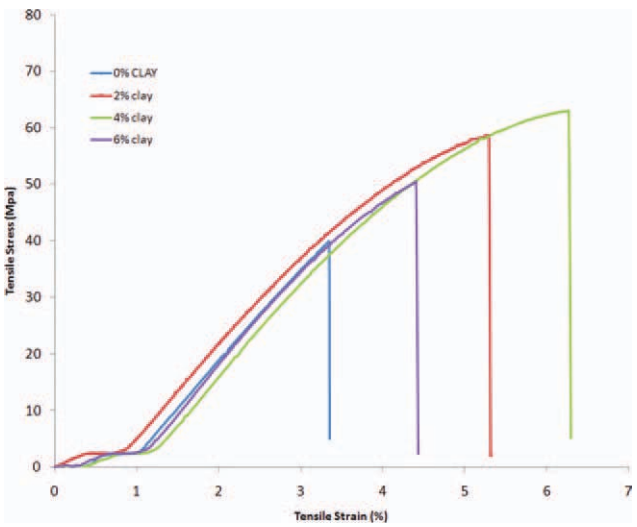

Figure 2 Stress–strain curves for the blends [50% N(6)/50% N(6,6)] containing 0, 2, 4, and 6 wt % nanoclay. [Color figure can be viewed in the online issue, which is available at wileyonlinelibrary.com.]

TABLE II
Mechanical Properties Deduced from the Nanoindentation Test of the Polymer Blends and Nanocomposites

Sample	Reduced modulus (GPa)	Elastic (Young's) modulus (MPa; nano)	Hardness (GPa; nano)
100% N(6)	1.844	1.621	0.179
4% clay	2.575	2.265	0.198
6% clay	4.701	3.376	0.311
100% N(6.6)	2.812	2.345	0.193
4% clay	3.495	2.917	0.204
6% clay	3.485	2.909	0.290
30% N(6)/70% N(6.6)	2.793	2.370	0.197
4% clay	3.387	2.875	0.223
6% clay	3.255	2.763	0.222
50% N(6)/50% N(6.6)	2.260	1.938	0.172
2% clay	2.037	1.746	0.163
4% clay	3.500	3.004	0.365
6% clay	3.668	3.149	0.352
70% N(6)/30% N(6.6)	2.527	2.190	0.201
4% clay	3.322	2.881	0.283
6% clay	3.775	3.274	0.341

decrease in the tensile strength for N(6,6) and the other mentioned blends.[2]

The elongation at break in N(6) decreased with increasing clay content. The decrease in the elongation at break with increasing clay content is a behavior reported for many polymer nanocomposites,[18–20] whereas in N(6,6) and the 50 wt % N(6)/50 wt % N(6,6) blend, an increase in the elongation at break at 4% clay loading happened; this indicated good ductility of the hybrid.[3] These increases in the ductility and elongation at break were followed by a decrease in the clay content at 6 wt % with a decrease also of the tensile strength, which indicated the inverse effect of the clay at higher clay loading (brittleness).

Indentation testing

The mechanical properties (reduced modulus E_r, elastic modulus, and hardness) obtained from the indentation test are summarized in Table II. The values reported here represent an average of four specimens for each sample, and each specimen underwent five cycles of loading and unloading. The elastic modulus, which was obtained from E_r with eq. (2), increased with increasing clay content for nearly all composites; this was the same behavior of the elastic modulus obtained by tensile testing. Comparing the values of the elastic modulus of the same composite obtained by the two different methods (tensile testing and indentation testing), we observed a difference, with greater values obtained by the indentation test. Possible origins for this difference, as reported by Dassari et al.,[21] were differences in the loading direction, local and bulk crystallinities, and crosslinking. The elastic modulus, measured by tensile testing for injection- and compression-molded specimens, differed from the direction in which it was measured during nanoindentation, and the presence of nanoparticles was expected to affect the polymer chain mobility and kinetics in their near vicinity and local chemistry at the interface. This caused different properties compared to those from the bulk.

The hardness, which quantifies the resistance of a material to plastic deformation, is shown in Figure 3, and it increased for nearly all of the composites with the addition of the nanoclay.

Thermal properties

The losses in weight for the neat N(6), N(6,6), their blends, and the nanocomposites were determined by TGA. $T_{90\%}$ and $T_{50\%}$, the maximum decomposition rate, and the residue for all of the composites are summarized in Table III. When the clay content was increased, all of the samples showed an increase in the residue over the neat composites, and most of them showed a decrease in the maximum decomposition rate (the maximum rate of weight loss) with increasing clay loading. $T_{90\%}$ and $T_{50\%}$ did not change considerably with the addition of clay, except in the 50 wt % N(6)/50 wt % N(6,6) blend and at 2 wt % clay loading; an improvement in the thermal properties of this blend was detected through an increase in $T_{90\%}$ from 408°C for the neat blend to 422°C and an increase in $T_{50\%}$ from 442 to 462°C. The maximum decomposition rate occurred at a higher temperature, 470°C, in comparison with that of the neat blend (450°C) and the other two clay loadings and with smaller values of maximum rate of weight loss (see Fig. 4); this indicated that the clay particles at this loading improved the thermal stability of the blend by acting as thermal insulators and mass transport barriers to the volatile products

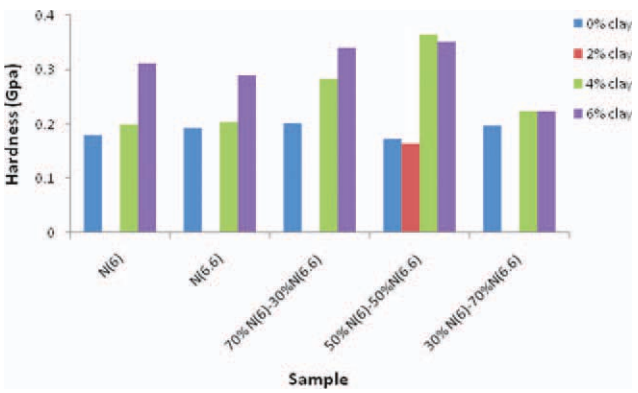

Figure 3 Hardness of the nanocomposites of N(6), N(6,6), and their blends obtained from nanoindentation. [Color figure can be viewed in the online issue, which is available at wileyonlinelibrary.com.]

TABLE III
TGA Results

Sample	$T_{90\%}$ (°C)	$T_{50\%}$ (°C)	Residue (%)	Maximum decomposition Rate (%/min)	Maximum decomposition Temperature (°C)
100% N(6)	400	445	0.7	22.6	450
4% clay	400	440	2.6	22.4	450
6% clay	400	440	4.6	21.4	450
100% N(6,6)	410	440	2.4	21.0	450
4% clay	410	445	4.9	18.5	450
6% clay	405	445	7.1	18.0	450
30% N(6)/70% N(6,6)	405	440	1.9	20.5	440
4% clay	404	445	4.6	17.1	450
6% clay	405	445	6.3	20.2	450
50% N(6)/50% N(6,6)	408	442	1.6	20.8	450
2% clay	422	462	2.6	18.1	470
4% clay	400	440	4.5	21.0	450
6% clay	400	440	5.8	21.2	450
70% N(6)/30% N(6,6)	402	443	1.2	21.5	450
4% clay	403	443	3.9	21.8	450
6% clay	402	445	4.5	22.3	450

generated during decomposition.[1,22,23] At a higher loadings of this blend beyond 2%, $T_{90\%}$ and $T_{50\%}$ decreased and then leveled off. This result was in agreement with those of Tiwari and Khilar,[11] who observed the maximum improvement in the thermal stability of their blend at 2 wt % clay loading, and those of Zhu et al.,[24] who obtained significant improvement of PS nanocomposites at a very low clay loading (0.1 wt %), and beyond 3 wt % clay, $T_{90\%}$ became nearly constant.

The effects of the nanoclay on the melting and crystallization temperatures of N(6), N(6,6), and their blends were examined by DSC. The thermal characterization results are given in Table I, which shows the maximum crystallization temperature (T_{cry}) and maximum melting temperature (T_m). Figure 5 represents the crystalization exothermic curves for N(6,6) nanocomposites, obtained from DSC cooling scans at a rate of 10°C/min. T_{cry} of the neat blends was less than that of neat N(6,6), and it decreased with the increase of N(6) loading; this indicated that the process of blending lowered T_{cry}. The crystallization process, which began spontaneously by polymer chain aggregation through a homogeneous nucleation mechanism, was delayed by the blending process, and this resulted in a decrease in the crystallization temperature in the blend below that of N(6) and N(6,6) to form stable nuclei for crystallization.

The addition of nanoclay increased T_{cry} of N(6,6) and the two blends 30 wt % N(6)/70 wt % N(6,6)

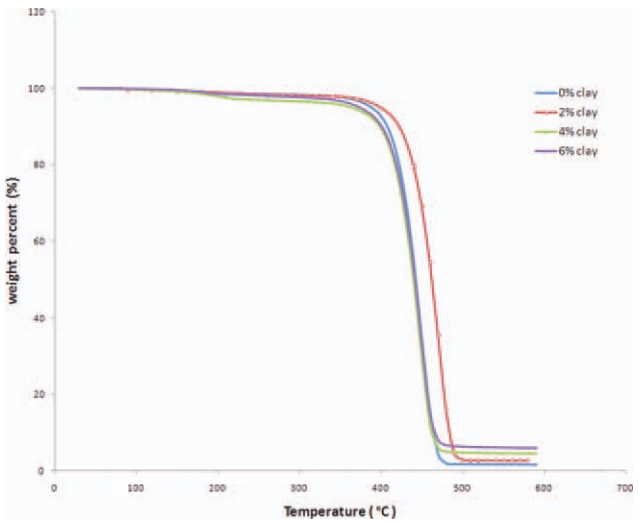

Figure 4 TGA thermograms of the blends [50% N(6)/50% N(6,6)] with different clay loadings. [Color figure can be viewed in the online issue, which is available at wileyonlinelibrary.com.]

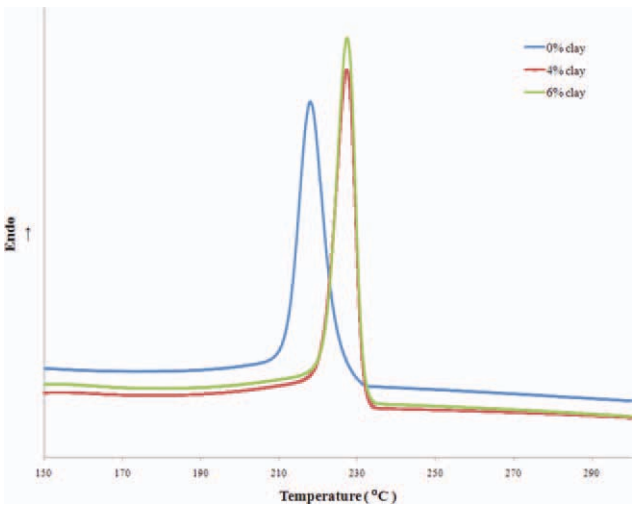

Figure 5 DSC cooling curves of the N(6,6) nanocomposites. [Color figure can be viewed in the online issue, which is available at wileyonlinelibrary.com.]

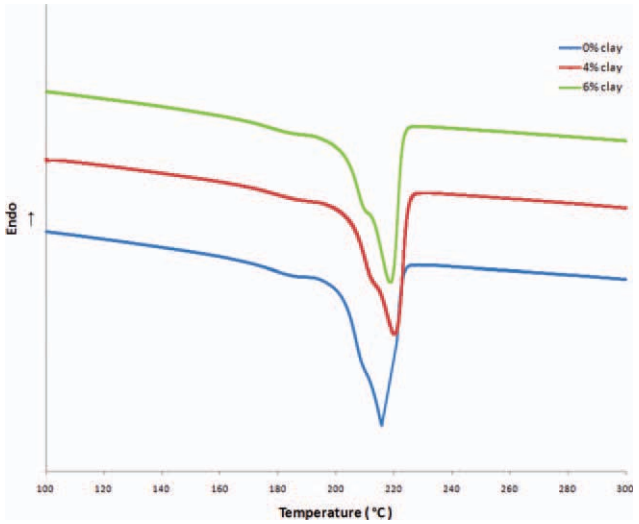

Figure 6 DSC heating curves of N(6) nanocomposites. [Color figure can be viewed in the online issue, which is available at wileyonlinelibrary.com.]

and 50 wt % N(6)/50 wt % N(6,6) by nearly 10, 5, and 10°C, respectively.

The clay particles acted as nucleating agents and increased the rate of crystallization. The neat composites crystallized by the homogeneous nucleation mechanism, as mentioned before, and that started spontaneously by polymer chain aggregation below the melting temperature.[2] Nanofillers act as nuclei to promote the crystallization process, which makes the chains order themselves at higher temperatures[5] and reduces the supercooling needed for crystallization. In the 50 wt % N(6)/50 wt % N(6,6) blend and beyond 2 wt % nanoclay loading, the rate of crystallization was retarded; this indicated good exfoliation of the clay at 2% loading, and this result was in full agreement with TGA, whereas in N(6) and the 70 wt

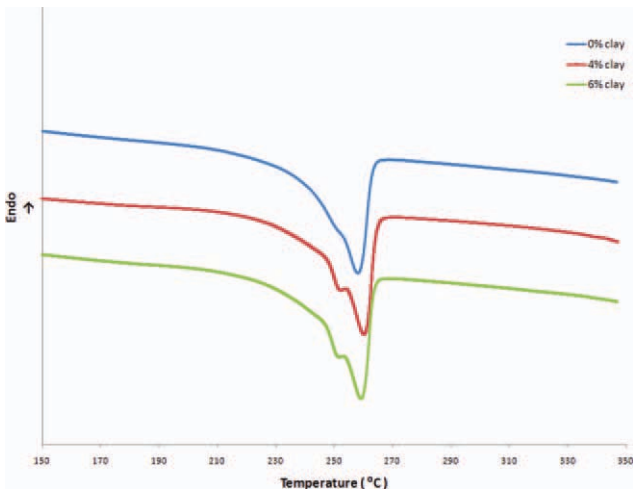

Figure 7 The DSC heating curves of N(6,6) nanocomposites. [Color figure can be viewed in the online issue, which is available at wileyonlinelibrary.com.]

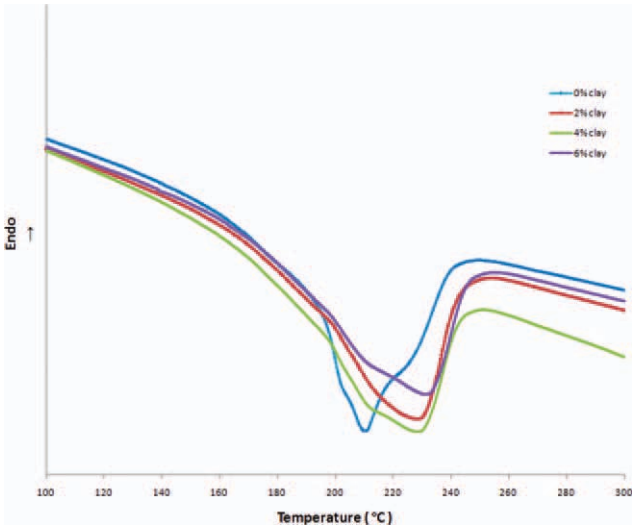

Figure 8 The DSC heating curves of (50% N(6)/50% N(6,6)) blend nanocomposites. [Color figure can be viewed in the online issue, which is available at wileyonlinelibrary.com.]

% N(6)/30 wt % N(6,6) blend, the crystallization temperature remained nearly constant, so the big improvement of Young's modulus in N(6) was a result of the nanoclay acting as a nanofiller and to strong hydrogen bonding interactions between the N(6) chains and the clay surfaces. FTIR spectroscopy showed a similar effect, as discussed later.

T_m of the neat blend [30 wt % N(6)/70 wt % N(6,6)] was between the T_m values of N(6) and N(6,6), whereas this temperature for the other two blends was less than those of N(6) and N(6,6) and the melting temperature as the crystallization temperature decreased with increasing N(6) loading.

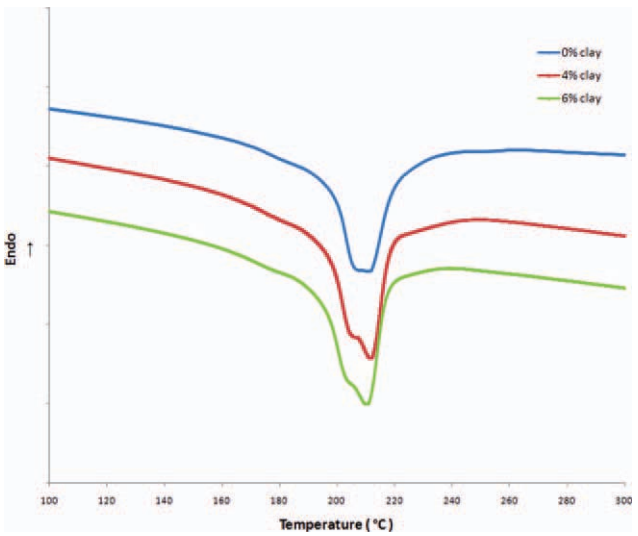

Figure 9 The DSC heating curves of (70% N(6)/30% N(6,6)) blend nanocomposites. [Color figure can be viewed in the online issue, which is available at wileyonlinelibrary.com.]

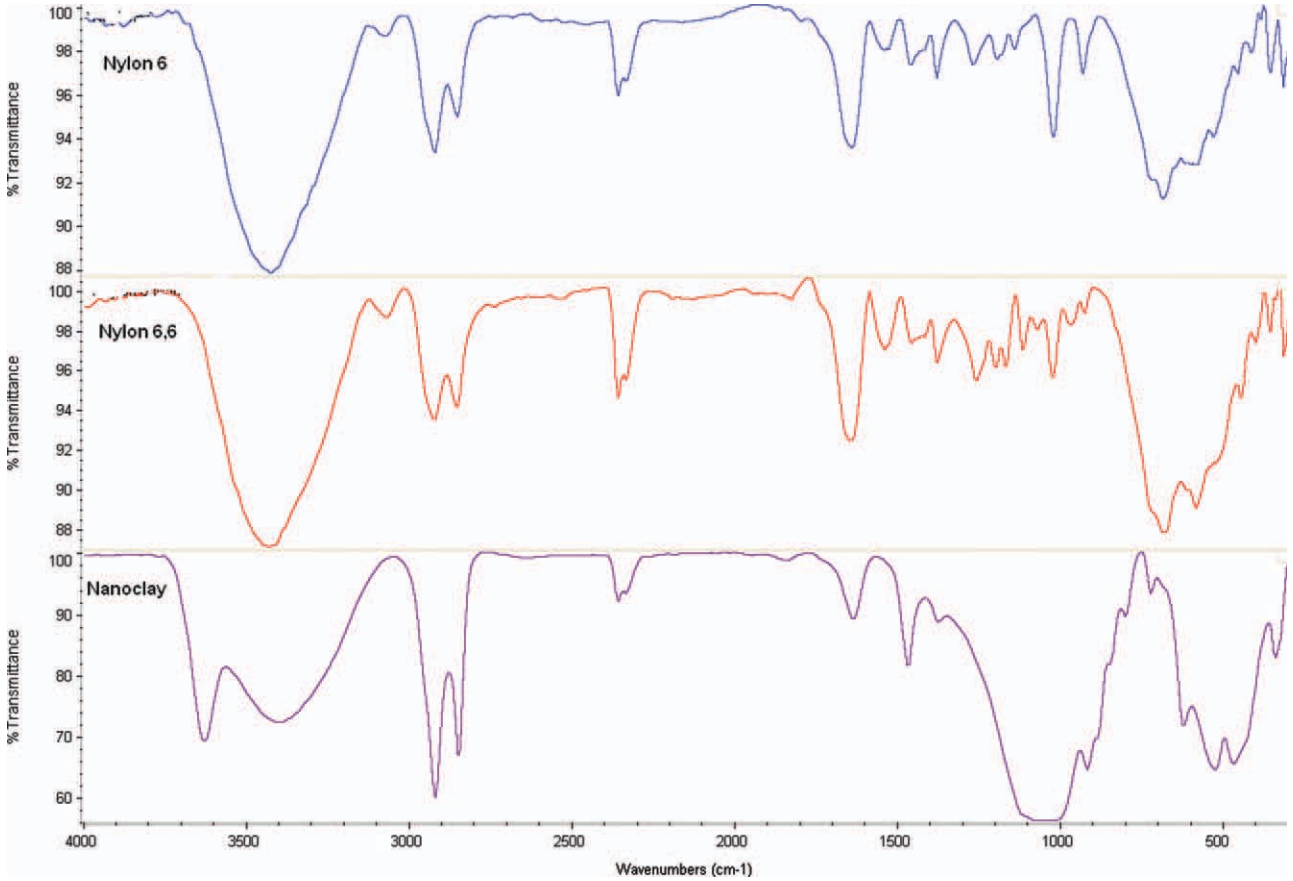

Figure 10 FTIR spectra of pure nanoclay, Nylon (6,6) and Nylon (6). [Color figure can be viewed in the online issue, which is available at wileyonlinelibrary.com.]

Figures 6–9 represent the melting endothermic curves of some of the nanocomposites obtained from the heating scans after cooling at the same rate of 10°C/min (some of the melting curves were shifted vertically for easier study). As shown in Table I, there was an increase of about 17–20°C in T_m for the 50 wt % N(6)/50 wt % N(6,6) blend after the addition of the nanoclay, and this was in full agreement with the improvement in the thermal properties of this blend according to the TGA, whereas the T_m values of N(6), N(6,6), and the other blends remained nearly constant after the addition of the clay; this consistency in the melting temperature has also been found in other systems.[25,26]

In N(6), N(6,6), and the 70 wt % N(6)/30 wt % N(6,6) blend, the addition of the clay enhanced the appearance of a small peak that appeared as a shoulder of the main melting peak. These two peaks in N(6), as reported by Sun et al.,[5] referred to the α-form crystals, which were thermodynamically stable and represented by the mean peak at nearly 220°C, and the other peak, which was as a shoulder of the mean peak, was due to the γ form at nearly 212–215°C. The two peaks in N(6,6) at 260 and 252°C were related to the α and β forms, respectively, as reported by Zhang[3] and Xin et al.[27] These two peaks' behavior in N(6,6) indicated that the clay could induce and enhance the β-form crystals, which appeared as a shoulder for the mean α peak, whereas for the 70 wt % N(6)/30 wt % N(6,6) blend, the melting temperature for the stable crystal structure was 210°C, and the melting temperature for the other crystal form was nearly 205°C. An acceptable theory for the two peaks' behavior was put forward by Roberts[28,29] and Holdsworth and Jones,[30] who said that the first peak, which appears as a shoulder for the mean peak, results from the melting of imperfect crystals and that the mean peak results from the melting of more perfect crystals, which results from the recrystallization of imperfect crystals heating.

FTIR characterization

FTIR spectroscopy was used to characterize the presence of specific chemical groups in the polymer material and to monitor any changes that may have occurred because of the blending process with nanoclay. It should be mentioned that the FTIR spectra were used as a qualitative measurement for the nanoclay blended with the N(6) and/or N(6,6) matrix, depending on the mixing ratios.

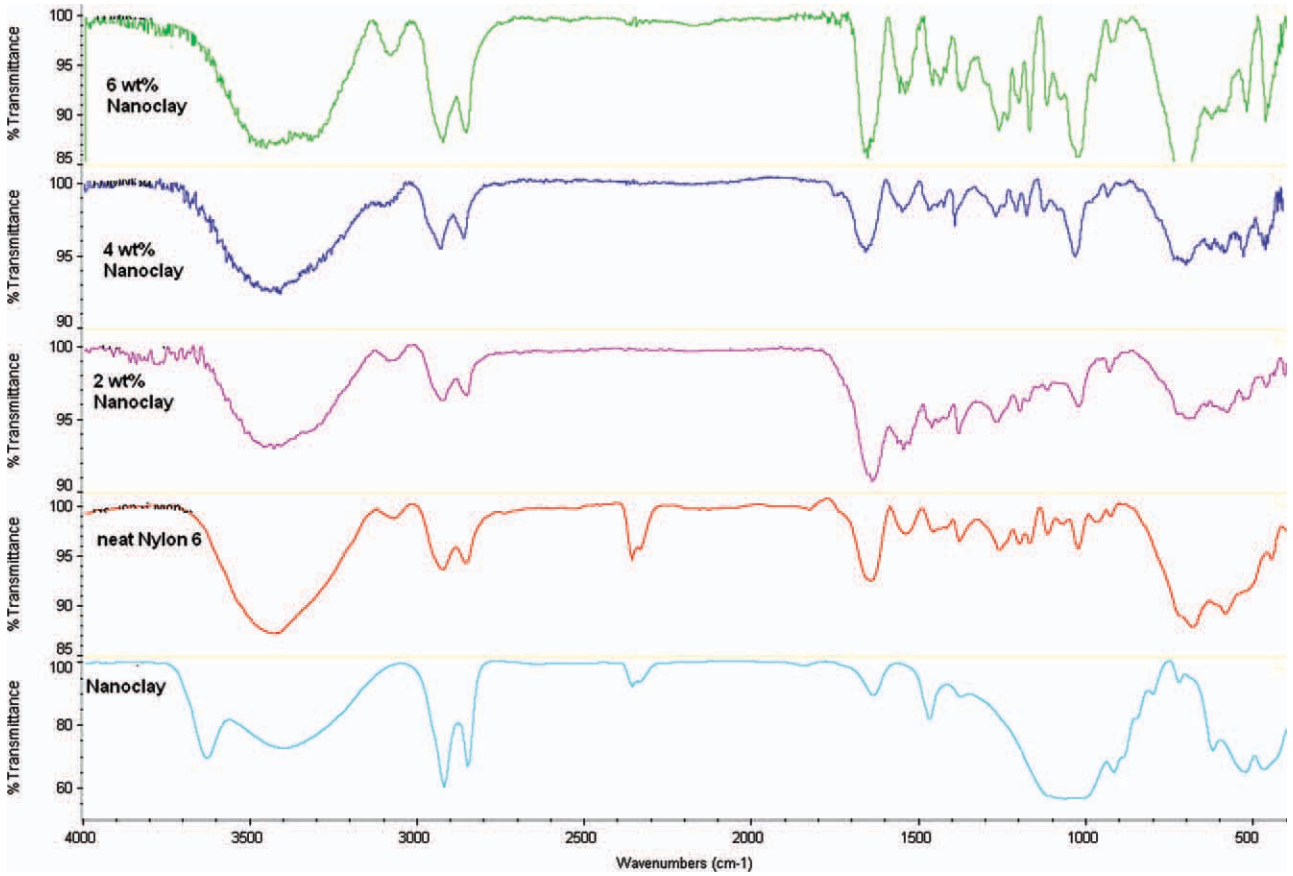

Figure 11 FTIR spectra of neat nanoclay, neat N(6) and varying weight percentage of nanoclay (i.e 0, 2, 4, and 6 wt% nanoclay in N(6). [Color figure can be viewed in the online issue, which is available at wileyonlinelibrary.com.]

To explain the extent of nanoclay incorporation in the polymer matrix and its effect on the mechanical properties of the polymer blends, the chemical structures of all of the samples were analyzed with FTIR spectroscopy.

In Figure 10, the FTIR spectra of pure N(6), N(6,6), and the nanoclay samples are presented. It clearly reveals the major bands associated with the two nylon samples. We observed C—H broad alkyl stretching bands at 2850–3000 cm^{-1}, typical strong carbonyl bands at 1650–1725 cm^{-1}, and a hydrogen-bonded band at 3400–3460 cm^{-1}. Intermolecular and intermolecular hydrogen bonding were expected to occur among the polymer chains because of the high hydrophilic forces between the NH and C=O groups present in both polymers.

The FTIR spectrum for pure nanoclay sample was also recorded as KBr disc, and its band assignments are presented as follows: the broad band centered near 3405 cm^{-1} was due to the —OH stretching band for interlayer water. The band at 3630 cm^{-1} was due to —OH group stretching for Al—OH and Si—OH. The shoulders and broadness of the structural —OH band were mainly due to contributions of several structural —OH groups occurring in the nanoclay. However, the position of the maximum of the band was clearly indicative of the chemical composition of the nanoclay. The characteristic peak at 1000–1125 cm^{-1} was due to Si—O stretching, and the transmittance peaks in the region of 1640 cm^{-1} were attributed to —OH bending mode in adsorbed water. The characteristic peaks at 1115 and 500 cm^{-1} were due to Si—O stretching (out of plane), and the peak at 500 cm^{-1} was due Si—O bending of the nanoclay. The IR peaks at 915, 875, and 836 cm^{-1} were attributed to AlAlOH, AlFeOH, and AlMgOH bending vibrations, respectively.[31–34]

Figure 11 shows the gradual increase in the intensities of the bands at 1640 cm^{-1}, which were present in both N(6) and N(6,6) and corresponded to carbonyl groups. The band at 500 cm^{-1}, corresponding to Si—O bending present in the nanoclay sample, supported the gradual changes in the composition of the polymer blend samples, which were related to the gradual increase of the weight fraction of the nanoclay content from 0 to 6 wt %.

In Figure 12, a few essential bands are considered to demonstrate the degree of nanoclay presence within the polymer matrix, the assignment of which was already discussed.

In this study, the primary motivation for determining the molecular structure of the polymer with

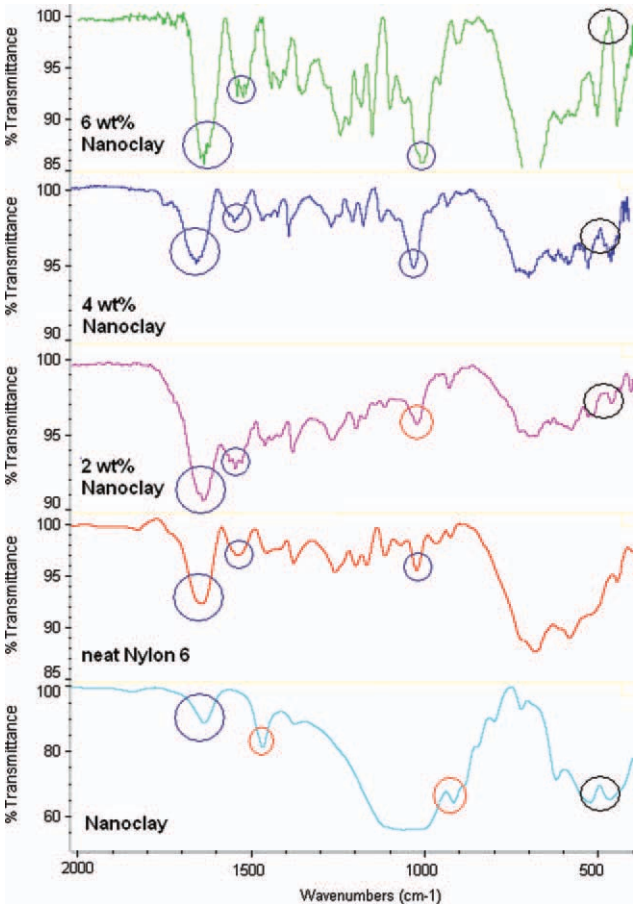

Figure 12 FTIR spectra of neat N(6), and varying weight percentage of nanoclay, namely 2, 4 and 6 wt%. [Color figure can be viewed in the online issue, which is available at wileyonlinelibrary.com.]

FTIR spectroscopy was to relate the structural changes to the performance properties. The enhancements in Young's modulus and hardness observed in the mechanical tests were due to the polar nature of both N(6) and N(6,6) and the possible formation of ionic bonds between the nanoclay and the polymer chains.[35,36]

XRD analysis

Nonuniformity or poorly dispersed regions in blends of nanoclay and nylon samples may occur because of either low concentration of the nanoclay or immiscibility between the polymer matrix and the nanoclay or any disorder present in the sample. When these samples are exposed to X-rays, useful information can be obtained and used to verify or refute these observations. The peak positions in the XRD patterns were used to derive the basal spacing of the nanoclay blended with various weight percentages of polyamides [i.e., N(6) and N(6,6)]. Figure 13 shows the XRD pattern of the neat N(6,6) and its

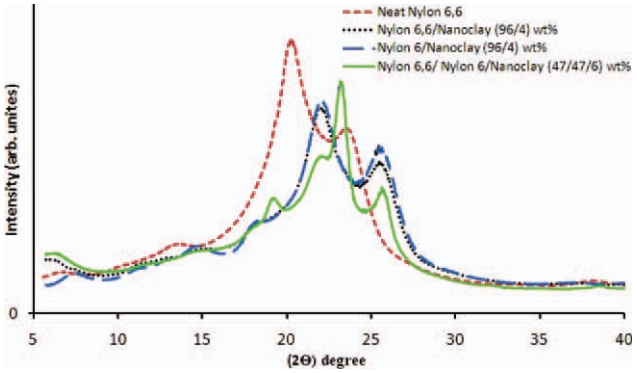

Figure 13 XRD patterns of the neat N(6,6) and its blends with N(6) and with 4 and 6 wt % nanoclay. [Color figure can be viewed in the online issue, which is available at wileyonlinelibrary.com.]

blends with various ratios of nanoclay and N(6). The powder diffractograms for neat N(6,6) showed two strong and well-resolved broad peaks at 2θ values around 20 and 24°; this indicated the existence of both forms of crystals, α_1 and α_2, respectively.[37,38] These two peaks could be clearly interpreted in confirming the α form of N(6,6). Because this was a pure sample with 0 wt % clay content, no peak appeared between 2θ values of 7–10, which are, according to Phang et al.,[39] associated with the presence of nanoclay. With increasing clay content or blending with N(6), no new peaks appeared in the XRD patterns at that region, and there was little change in the relative intensities of the α_1 and α_2 peaks for all of the samples. This observation indicated that the clay did not induce new crystalline forms in N(6,6) and did not interrupt the crystalline structure of the α form.

The reduction in the intensity of the two peaks and the shift to higher 2θ values (22 and 26°) for N(6,6) with 4 wt % nanoclay resulted from the decrease in the amount of intercalated clay; it suggested the breakdown of platelet agglomerates or partial exfoliation. Consequently, the clay platelets were uniformly dispersed in the polymer matrix rather than agglomerated as tactoids.[40]

For all samples containing various weight percentages of nanoclay, there was no well-resolved peak associated with the nanoclay at $2\theta < 10°$. This indicated that most of the nanoclay was well dispersed within the polymer.

CONCLUSIONS

Nanocomposites of N(6), N(6,6), and their blends [30 wt % N(6)/70 wt % N(6,6), 50 wt % N(6)/50 wt % N(6,6), and 70 wt % N(6)/30 wt % N(6,6)] at different clay loadings were prepared by the mixture of the polymers with an organically modified clay, 1.34TCN, compatible with the polymer matrix

(nylons). The mix was melted and injected into strip-shaped samples. The mechanical results show increases in the Young's moduli, which were obtained from the tensile testing, for all of the nanocomposites, with the greatest increase in N(6) of nearly 55% above that of the neat sample, whereas the enhancement in the tensile strength depended on the blend ratio and had its greatest effect on the 50 wt % N(6)/50 wt % N(6,6) blend. This blend exhibited ductile behavior after the addition of 2 and 4 wt % clay. The reduced modulus and elastic modulus obtained from the indentation test and calculated by the Oliver–Pharr method showed increases after the addition of the clay, which was the same behavior as that of Young's modulus obtained from the tensile test but with greater values due to different loading directions and differences in the local and bulk crystallinities and crosslinking. The TGA results show an improvement in thermal properties of the 50 wt % N(6)/50 wt % N(6,6) blend through increases in $T_{90\%}$ and $T_{50\%}$, from 408 and 442°C for the neat blend to 422 and 462°C at 2 wt % clay loading. The maximum decomposition rate occurred at a higher temperature, 470°C, in comparison with that of the neat blend, at 450°C. DSC showed increases in the crystallization temperature for N(6,6) and the two blends 30 wt % N(6)/70 wt % N(6,6) and 50 wt % N(6)/50 wt % N(6,6) in addition to the enhancement of the two-peak melting behaviors in N(6), N(6,6), and the 70 wt % N(6)/30 wt % N(6,6) blend after the addition of the clay. The enhancement in the Young's modulus and hardness observed in mechanical tests were supported by FTIR spectroscopy, and we concluded that this was because of the polar nature of both N(6) and N(6,6), which contributed to the formation of hydrogen bonding and most likely the formation of ionic bonds between the nanoclay and the polymer chains.

References

1. Gyoo, P. M.; Venkataramani, S.; Kim, S. C. J Appl Polym Sci 2006, 101, 1711.
2. Biqiong Chen, A.; Julian, R. G.; Evans, B. Polymer 2008, 49, 5113.
3. Zhang, X.; Loo, L. S. J Polym Sci Part B: Polym Phys 2008, 46, 2605.
4. Wu, M. T.; Chen, E. C. Polym Eng Sci 2002, 42, 1141.
5. Sun, L.; Yang, J. T.; Lin, G. Y.; Zhong, M. Q. Mater Lett 2007, 61, 3963.
6. Samal, S. K.; Mohanty, S.; Mohanty, S. J Thermoplast Compos Mater 2008, 21, 243.
7. Leuteritz, A.; Pospiech, D.; Kretzschmar, B.; Willeke, M.; Jehnichen, D.; Jentzsch, U.; Grundke, K.; Janke, A. Adv Eng Mater 2003, 5, 678.
8. Zheng, X.; Jiang, D. D.; Wilkie, A. C. Polym Degrad Stab 2006, 91, 108.
9. Jin, H. S.; Chang, J. H. Fibers Polym 2007, 8, 451.
10. Wait, M. U.; Hassan, A.; Rahmat, A. R.; Lim, J. W.; Ishak, Z. A. J Reinf Plast Compos 2006, 25, 933.
11. Tiwari, R. R.; Khilar, K. C. J Appl Polym Sci 2008, 108, 1818.
12. Frounchi, M.; Dadbin, S.; Salehpour, Z.; Noferesti, M. J Membr Sci 2006, 282, 142.
13. Oliver, W. C.; Pharr, G. M. J Mater Res 1992, 7, 1564.
14. Shuman, D. J.; Costa, A. L. M.; Andrade, M. S. Mater Characterization 2007, 58, 380.
15. Oliver, W. C.; Pharr, G. M. J Mater Res 2004, 19, 3 (review article).
16. Fornes, T. D.; Yoon, P. J.; Hunter, D. L.; Keskkula, H.; Paul, D. R. Polymer 2002, 43, 5915.
17. Gorrasi, G.; Tortora, M.; Vittoria, V.; Galli, G.; Chellini, E. J Polym Sci Part B: Polym Phys 2002, 40, 1118.
18. Tjong, S. C.; Meng, Y. Z.; Hay, A. S. Chem Mater 2002, 14, 44.
19. Tjong, S. C.; Meng, Y. Z.; Xu, Y. J Polym Sci Part B: Polym Phys 2002, 40, 2860.
20. Yoon, P. J.; Hunter, D. L.; Paul, D. R. Polymer 2003, 44, 5323.
21. Dassari, A.; Yu, Z. Z.; Mai, Y. W. Mater Sci Eng 2009, 63, 31.
22. Noh, M. H.; Jang, L. W.; Lee, D. C. J Appl Polym Sci 1994, 74, 179.
23. Zanetti, M.; Camino, G.; Thomann, R.; Mülhaupt, R. Polymer 2001, 42, 4501.
24. Zhu, J.; Morgan, A. B.; Lamlas, F. J.; Wilkie, C. A. Chem Mater 2001, 13, 3774.
25. Chang, J. H.; Sung, J. K.; Yong, L. J.; Im, S. Polymer 2004, 45, 919.
26. Park, B. J.; Kim, T. H.; Choi, H. J.; Lee, J. H. J Macromol Sci B 2007, 46, 341.
27. Xin, K.; Suqin, H.; Chengshen, Z.; Liyun, L.; Jiangue, G. J Appl Polym Sci 2005, 95, 756.
28. Roberts, R. C. Polymer 1969, 10, 117.
29. Roberts, R. C. J Polym Sci Part B: Polym Lett 1970, 8, 381.
30. Holdsworth, P. J.; Jones, T. A. Polymer 1971, 12, 195.
31. Madejova, J. Vib Spectrosc 2003, 31, 1
32. Patel, H. A.; Somani, R. S.; Bajaj, H. C.; Jasra, R. V. Ind Eng Chem Res 2010, 49, 1677.
33. Patel, H. A.; Somani, R. S.; Bajaj, H. C.; Jasra, R. V. Bull Mater Sci 2006, 29, 133.
34. Xi, Y.; Ding, Z.; Hongping, H.; Frosr, R. L. Spectrochim Acta Part A 2005, 61, 515.
35. Kojima, Y.; Usuki, A.; Kawasumi, M.; Okada, A.; Kurauchi, T.; Kamigaito, O. J Polym Sci Part A: Polym Chem 1993, 31, 983.
36. Kojima, Y.; Usuki, A.; Kawasumi, M.; Okada, A.; Kurauchi, T.; Kamigaito, O. J Polym Sci Part A: Polym Chem 1993, 31, 1755.
37. Lu, Y.; Zhang, Y.; Zhang, G.; Yang, M.; Yan, S.; Shen, D. Polymer 2004, 45, 8999.
38. Li, Y.; Hu, X. J Polym Sci Part B: Polym Phys 2007, 45, 1494.
39. Phang, I. Y.; Chen, L.; Tjiu, W. C.; Pisharath, S.; Liu, T. X. Mater Res Innov 2004, 8, 159.
40. Shen, L.; Phang, I. Y.; Chen, L.; Liu, T.; Zeng, K. Polymer 2004, 45, 3341.